Available online at www.sciencedirect.com
ScienceDirect
Journal of the European Ceramic Society 29 (2009) 2143–2152
www.elsevier.com/locate/jeurceramsoc

High-alumina porcelain with the addition of a Li_2O-bearing fluxing agent

M. Oberžan [a,*], J. Holc [b], M. Buh [b], D. Kuščer [b], I. Lavrač [a], M. Kosec [b,c]

[a] *ETI d.d, Obrezija 5, 1411 Izlake, Slovenia*
[b] *Institut Jožef Stefan, Jamova 39, 1000 Ljubljana, Slovenia*
[c] *Jožef Stefan International Postgraduate School, Jamova 39, 1000 Ljubljana, Slovenia*

Received 3 November 2008; received in revised form 26 January 2009; accepted 28 January 2009
Available online 24 February 2009

Abstract

We have studied the influence of increasing the amount of β-spodumene ($LiAlSi_2O_6$), as a Li_2O-containing flux, on the phase composition, the microstructure evolution and the physical properties of high-alumina porcelain. Quartz reacts with β-spodumene in the temperature range 1150–1250 °C, forming lithium aluminium silicates with a larger amount of SiO_2. The presence of lithium minerals contributes to a lower CTE for the fired bodies. At 1300 °C an improved flexural strength is achieved with compositions containing 1.0 or 1.2 wt.% of Li_2O, as a result of a more uniform microstructure. With increasing amounts of Li_2O the overfiring effect is greatly enhanced. The most favourable characteristics from an industrial perspective with regard to flexural strength and deformation during firing were attained by using a high-alumina porcelain composition containing 1.0 wt.% Li_2O.

Keywords: Porcelain; Spodumene; Sintering; Strength; Thermal expansion

1. Introduction

Technical porcelains, which are classified in the alkaline alumina silicate porcelain group, find diverse application in electrotechnics, most often as the insulating parts in electricity transmission, distribution and protection. The developments in electrical engineering dictate the need for technical porcelains with high reliability, and it has been shown that the reliability of porcelain strongly depends on the microstructure and phase composition.[1,2] The typical requirements for an electrical porcelain are a high mechanical strength and a good thermal shock resistance. To achieve a better mechanical strength for the porcelain body, alumina with its higher Young's modulus is used instead of quartz as a filler.[3,4] This increasing amount of alumina greatly contributes to the strength enhancement, but at the same time causes the thermal expansion to increases, thus reducing the thermal shock resistance. Therefore, to reduce the expansion of high-alumina porcelain it is necessary to reduce the expansion of the glassy phase or introduce low-expansion phases.

The viscous liquid that is formed during the firing of the porcelain body enables densification and the formation of the final microstructure.[5] The temperatures at which this liquid is formed are lowered by the introduction of flux, with sodium- and potassium-based feldspars being the most commonly used fluxes in porcelain. It has also been reported that a combination of feldspar and nepheline syenite contributes to the increased mechanical strength of porcelain bodies.[6] The level of vitrification, the pyroplastic deformation and the microstructure are affected by the mineralogical composition of the raw materials and by the level of equilibrium achieved.[7]

The use of lithium-bearing minerals as a liquid-phase sintering aid has been investigated in various types of ceramics. It was reported that spodumene as a partial replacement for feldspar can lower the firing temperature of sanitary chinaware bodies with a high content of flux when the feldspar-to-spodumene ratio is 70:30.[8] Bodies of electrical porcelain with a fairly high thermal shock resistance and mechanical strength were developed using 18.5–20.5 wt.% of spodumene and firing at 1380 °C.[9] Good properties for tableware porcelains were attained when the Li_2O content did not exceed 1.5 wt.%, and these compositions matured at temperatures 100–120 °C lower than standard, triaxial porcelain formulations.[10] The presence of spodumene, when 10 wt.% was added as a partial replacement for sodium feldspar,

* Corresponding author.
E-mail address: martina.oberzan@eti.si (M. Oberžan).

0955-2219/$ – see front matter © 2009 Elsevier Ltd. All rights reserved.
doi:10.1016/j.jeurceramsoc.2009.01.029

reduced the firing temperature and the shrinkage of the body mixes for stoneware tiles.[11] The use of lithium-bearing minerals as a liquid-phase sintering aid has also been investigated in other types of ceramics, for example, in mullite ceramics,[12,13] to lower the firing temperature and in alumina ceramics[14] to improve the thermal shock resistance. The influence of a Li_2O-bearing fluxing agent in a high-alumina porcelain body has not yet been investigated.

The aim of our work was to investigate the influence of Li_2O in combination with K_2O as a flux on the sintering behaviour and the physical properties of high-alumina porcelain bodies. The increasing amounts of Li_2O were introduced in compositions via a commercial spodumene concentrate. The investigations were assisted by a study of the phase composition and the microstructural development at different firing temperatures. All the characteristics were compared with an alumina porcelain body containing K_2O and Na_2O as the flux. New body formulations, suitable for extrusion and industrial applications, were developed.

2. Materials and experimental procedure

We compared the reference formulation (EN) with three model formulations (A, B, and C) of high-alumina porcelain. The model formulations were prepared using calcined alumina (HVA, Almatis GmbH, D), kaolin (Zettlitz Ia, Sedlecký kaolin a.s., CZ), illite clay (M1M, Stephan Smidt, D), bentonite (Portaclay A, Ankerpoort NV, NL), calcined spodumene (SC 7.5, Gwalia Consolidated Ltd, Australia) and potassium feldspar (Dorkasil 90, Dorfner, D). Additionally, 0.3 wt.% of binder based on polyvinyl alcohol was admixed to improve the plasticity for extrusion.

Conventional ceramic processing routes were used to prepare the model alumina porcelain bodies on a laboratory scale. First, the materials were wet milled with alumina balls for around 11 h. The particle size and the particle size distribution after milling were measured by laser sedigraph (Matroc Microtrac S3500). The distribution for all the model compositions was bimodal, with the first maximum around 0.6 μm and the second one between 3 and 4 μm. The EN reference composition was milled in an industrial mill with silica balls, and its particle size distribution was comparable to that of the model compositions.

Suspensions of the milled model compositions A, B and C were dried on plaster moulds at room temperature. The EN suspension was spray dried and mixed with water in a Z-mixer. Test samples in the form of extruded circular bars were prepared on a laboratory vacuum-extrusion machine (Netzsch, V5). The samples were dried for one day at room temperature followed by 4 h drying in an oven at 105 °C.

The samples were fired in a laboratory electric furnace (Naber N20/14) in the temperature range 950–1350 °C or in a gas kiln. Before firing the test samples were set in refractory saggars. In the laboratory furnace the firing process involved a 4 °C/min heating rate and a 15-min soaking time, and was the same for each firing, except for the maximum temperature. The seven different maximum temperatures were 950, 1050, 1150, 1200, 1250, 1300 and 1350 °C. After soaking at the maximum temperature the samples were cooled to room temperature at the natural rate for the laboratory furnace. In the gas kiln the firing was carried out at a maximum temperature of 1315 °C and the duration of the complete firing cycle was 11 h. The atmosphere was changed during the firing cycle, with oxidation up to 1100 °C, followed by reduction until the end of the firing at the maximum temperature. The cooling process was in an oxidising atmosphere.

Characterization of the investigated high-alumina porcelain bodies after firing involved both physical and structural characterizations. The physical characterization included assessments of the open porosity, the bulk density, and the thermal and mechanical properties. The structural characterization included measurements of the phase composition and the microstructure.

The bulk density and the open porosity were measured using the standard method, in accordance with the IEC 60672-2 standard [15] with deionized water as the immersion medium. Two samples of half-cut test bars, Ø10 × 120 mm, were used for the open-porosity and bulk-density measurements.

The behaviour of the samples during heating was assessed from the DTA and TG curves, which were recorded on powdered mixtures in the temperature range 25–1200 °C (Netzsch STA 429, 5 °C/min), and from sintering curves recorded on test samples in the form of bars Ø7 × 25 mm in the temperature range 20−1340 °C using a dilatometer (Baehr, heating rate 5 °C/min). The linear thermal expansion and the corresponding curves of the coefficient of thermal expansion (CTE) were measured on fired test bars, Ø6 × 50 mm, using a dilatometer (Netzsch DIL 402EP, heating rate 5 °C/min) in the temperature range 30−980 °C. The thermal shock evaluations were determined in accordance with the IEC 60672-2 standard.[15] The deformation of the samples during firing in a gas kiln was measured as the height reduction of the test bars relative to a horizontal surface. The test bars, Ø10 × 180 mm, were positioned on a refractory support with a height of 100 mm and a span of 150 mm. Five test bars were measured to evaluate the deformation during firing.

The flexural strength was determined on circular test bars, Ø10 × 120 mm, using a three-point bend tester (Netzsch 401/3) with a 100-mm span. Seven test bars were used for each set of measurements. The maximum and minimum values were eliminated from the results, thus the flexural strength was calculated as the average of five measured values.

The phase composition was studied from X-ray powder-diffraction (XRD) patterns recorded on powdered samples (<63 μm) at room temperature (PANalytical, X'Pert PRO MPD, The Netherlands) using Cu-Kα radiation. The data were collected in the 2θ range from 10 to 70°, in steps of 0.034°, with an integration time of 100 s. The crystal phases were identified using a complete ICDD powder pattern file and the X'Pert PC software. The microstructure was observed using optical and scanning electron microscopy (SEM, JEOL 5800 equipped with an energy-dispersive X-ray analyzer (EDX)). The samples for the microstructure observation were cut from Ø10-mm test bars with a cross-sectional orientation and prepared by grinding and polishing using standard metallographic techniques. Prior to any analysis in the SEM, the samples were coated with carbon to provide the electrical conductivity.

Table 1
Chemical composition of fired reference (EN) and model (A, B and C) formulations (wt.%).

Oxide	EN	A	B	C
SiO_2	34.34	34.34	33.76	34.27
Al_2O_3	60.51	61.15	61.68	60.87
Fe_2O_3	0.33	0.44	0.42	0.36
MgO	0.31	0.13	0.13	0.12
CaO	0.23	0.13	0.14	0.12
Na_2O	0.66	0.17	0.19	0.20
K_2O	2.98	1.96	1.86	1.90
TiO_2	0.20	0.20	0.16	0.13
Li_2O	–	1.02	1.18	1.56

3. Results and discussion

The chemical compositions of the fired reference and model formulations are presented in Table 1, from which it is clear that they are all relatively similar in terms of the types and quantities of the oxides, except for the alkali oxides. In the compositions A, B, and C, Na_2O and to some extent K_2O were replaced with the increasing amount of Li_2O. The reference composition EN, as an industrial composition, is characterized by its higher Na_2O and K_2O content.

The DTA and TG curves of the reference body EN and the Li_2O-containing bodies A, B and C are shown in Fig. 1. In the DTA curves an endothermic effect is observed, with its maximum at ~525 °C for the samples EN, A and B, and at ~518 °C for sample C. An exothermic effect appears, with its maximum ~985 °C for EN and at ~970 °C for the samples containing Li_2O. In the TG traces the weight loss up to 400 °C is about 1%, for all the samples. In the heating range 400–800 °C the weight loss values for EN, A, B and C are 3.6%, 3.9%, 3.5% and 3.0 %, respectively. When the samples were heated from 800 to 1200 °C they all exhibited only about 0.2% weight loss.

It is evident from the DTA and TG curves that similar reactions take place in all the samples up to 1200 °C. Both the endothermic and exothermic effects observed in the DTA curves are characteristic for the kaolinite-to-mullite reaction series, with the endothermic dehydroxylation reaction of kaolinite in the range 450–600 °C, completed at about 900 °C, and

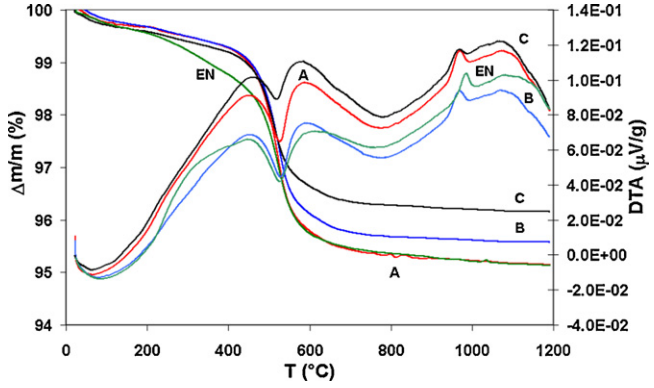

Fig. 1. DTA and TG curves of studied compositions recorded in the temperature range 25–1200 °C.

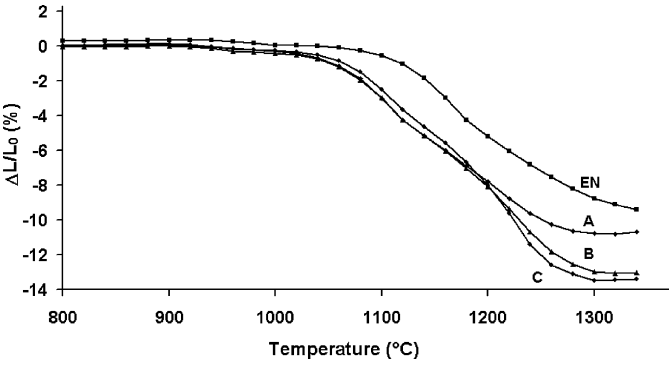

Fig. 2. Sintering curves of studied compositions recorded in the temperature range 800–1340 °C.

an exothermic reaction in the range 800–1000 °C, when mullite begins to form from metakaolinite.[16,17,18] The addition of Li_2O enhances the mullite formation since the maximum of the exothermic effect in the temperature range 800–1000 °C is 15 °C lower for the samples containing Li_2O than for the reference composition. The weight loss is related to the quantity of clay constituents. The weight loss is the lowest for composition C, which contains the smallest quantity of clay constituents. As confirmed by the DTA and TG curves, the main reactions that occur up to 1000 °C are attributed to the clay constituents and their quantities in the samples.

3.1. Sintering behaviour of the studied bodies

The sintering curves in Fig. 2 show the dimensional changes of the samples as a function of temperature in the range 800–1340 °C. In temperature range up to 1000 °C the curves of the compositions A, B and C overlap, while the reference composition, EN, which has a similar trend, lies slightly above. The comparable dilatation behaviour in all the samples up to 1000 °C is attributed to the similar reactions that take place, as confirmed by the DTA curves. The onset temperature of intensive shrinkage is 1060 °C, for A, B and C, and 1110 °C, for EN. The maximum shrinkage values for the compositions A, B and C are 10.8%, 13.1% and 13.5%, respectively. The compositions A and B achieve their maximum shrinkage at the same temperature, 1320 °C, while C completes its shrinking at 1300 °C. The reference composition, EN, attains a shrinkage of 9.4 % at 1340 °C, with its sintering curve still in decline, indicating that the shrinkage continues above 1340 °C. Above the temperature of maximum shrinkage, expansion is observed for all the compositions containing Li_2O, which is indicated by the bloating of the bodies.

The results show that the densification process of the bodies is enhanced by the presence of Li_2O, in a similar way to that reported for triaxial porcelain bodies[10] and bodies for porcelain stoneware tiles.[11]

3.2. Phase composition and microstructure evolution

Before implementing the firing cycles at increasing temperatures, the mineralogical composition of the green bodies

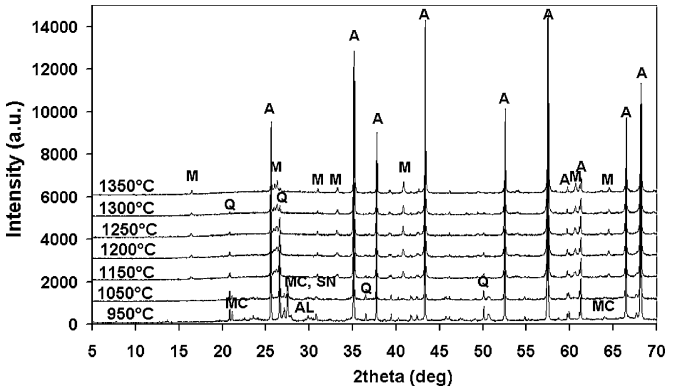

Fig. 3. XRD patterns of reference composition EN fired in temperature range 950–1350°C. Identified minerals are: α-alumina (A), mullite (M), α-quartz (Q), microcline (MC), sanidine (SN) and albite (AL).

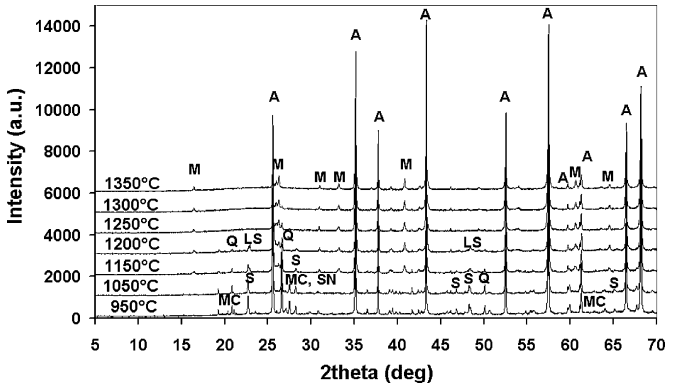

Fig. 4. XRD patterns of composition A fired in the temperature range 950–1350°C. Identified minerals are: α-alumina (A), mullite (M), α-quartz (Q), microcline (MC), sanidine (SN), β-spodumene (S) and $LiAlSi_3O_8$ (LS).

was identified from the XRD patterns of powdered, extruded samples, with the aim to assist the phase interpretation of the fired samples. In all the green bodies, corundum (α-Al_2O_3) prevailed as the primary mineral phase. However, kaolinite ($Al_2Si_2O_5(OH)_4$), microcline ($KAlSi_3O_8$) and α-quartz (SiO_2) were also present in all the green bodies. The kaolinite came from the clay part, the microcline was present as the main mineral in potassium feldspar, and the presence of α-quartz (SiO_2) is the result of quartz being the accompanying mineral for clays and fluxes. Albite ($NaAlSi_3O_8$) was only identified in the reference composition, EN, where the flux system consisted of potassium and sodium feldspar. β-Spodumene ($LiAlSi_2O_6$) was only present in the model compositions A, B and C, where it was added as the main flux component.

The temperature range from 950 to 1350 °C was selected for investigating the phase composition and the microstructure development due to the major shrinkages observed in this range from the sintering curves in Fig. 2. It was divided into seven firing temperatures, with closer temperature intervals in the region of sintering curves where the rate of densification was the greatest.

Fig. 3 presents the XRD spectra of the composition EN fired at different temperatures. Corundum, as the predominating crystalline phase, is observed in all the fired samples. The phases in addition to corundum in the samples fired at 950 and 1050 °C are the flux minerals microcline, sanidine and albite, with their peak intensities decreasing with increasing temperature up to 1150 °C, at which point they disappear. The intensity of the α-quartz peaks gradually diminishes with increasing temperature, indicating its partial dissolution in the feldspar melt. However, the α-quartz is still present at 1350 °C, and the mullite is formed at 1150 °C. The process of mullitization continues with increasing temperature, which is clear from the increasing intensities of the mullite peaks. The phase composition and the phase-transformation process of the EN material is comparable with the processes occurring in a typical triaxial porcelain body, [1,16,18,19] except that corundum, as the main phase, is additionally present at all the firing temperatures.

Fig. 4 presents the phase development with temperature for sample A. It is clear that corundum prevails in all the samples. The flux minerals microcline and sanidine were identified at

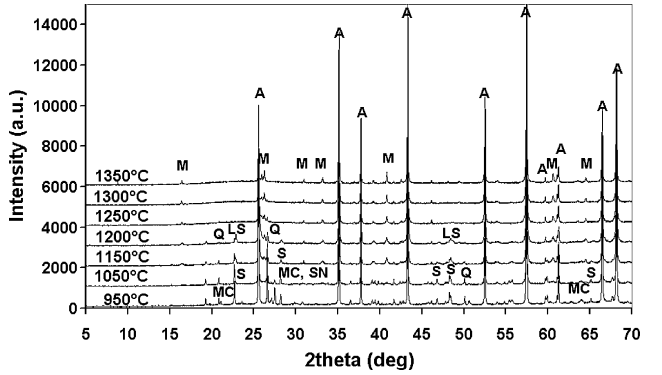

Fig. 5. XRD patterns of composition B fired in the temperature range 950–1350°C. Identified minerals are: α-alumina (A), mullite (M), α-quartz (Q), microcline (MC), sanidine (SN), β-spodumene (S) and $LiAlSi_3O_8$ (LS).

950 and 1050 °C. β-$LiAlSi_2O_6$ (JCPDS 071-2058) is detected up to 1200 °C, and at 1150 and 1200 °C $LiAlSi_3O_8$ (JCPDS 035-0794) coexists with β-$LiAlSi_2O_6$. In contrast, α-quartz is identified at all temperatures. However, the amount of α-quartz decreases with temperature faster than for the EN, suggesting that the dissolving of α-quartz is enhanced by the presence of Li_2O. Mullite is first detected at 1150 °C, and its amount increases with temperature.

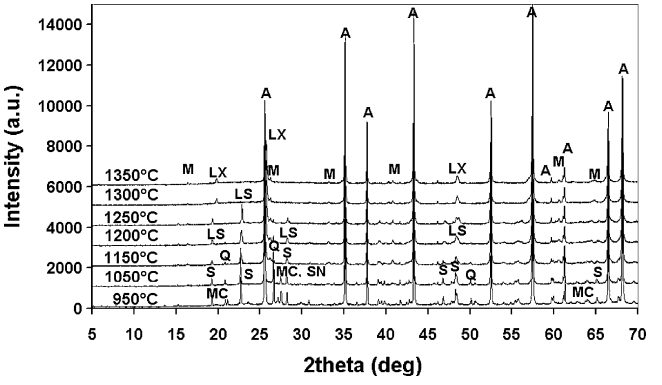

Fig. 6. XRD patterns of composition C fired in the temperature range 950–1350°C. Identified minerals are: α-alumina (A), mullite (M), α-quartz (Q), microcline (MC), sanidine (SN), β-spodumene (S), $LiAlSi_3O_8$ (LS) and $Li_xAl_xSi_{1-x}O_2$ (LX).

In Fig. 5 the occurrence of phases in sample B at different temperatures is shown. The phase compositions of A and B are identical at all the firing temperatures, except that at 1350° the α-quartz cannot be detected in B, suggesting that the increasing amount of Li_2O tends to enhance the dissolution of the α-quartz.

Fig. 6 shows the phase evolution during the heating of sample C. The minerals identified in C are different to those in A and B in the temperature range above 1200 °C, since $LiAlSi_3O_8$ is still detected at 1250 °C, while at 1300 and 1350 °C the new Li-containing phase, $Li_xAl_xSi_{1-x}O_2$ (JCPDS 040-0073), is identified. The α-quartz disappears at temperatures below 1300 °C.

In Li_2O-containing compositions the dissolution of microcline and sanidine is similar to the case of EN, indicating that the presence of β-spodumene has no perceivable effect on the breakdown of sanidine and microcline below 1150 °C. The amount of β-spodumene decreases with increasing temperature up to 1250 °C. Simultaneously, at 1150 °C, the Li-containing phase with a larger amount of SiO_2, i.e., $LiAlSi_3O_8$, is formed, which is correlated with the decreasing amount of α-quartz. The reactions of lithium minerals at temperatures above 1200 °C are affected by the amount of Li_2O. In A and B, with 1.0 and 1.2 wt.% Li_2O, respectively, $LiAlSi_3O_8$ is only identified at 1150 and 1200 °C; at higher temperatures it appears to have melted in the feldspathic liquid, since none of the Li-minerals is detected at 1250 °C or above. In C, with 1.6 wt.% of Li_2O, $LiAlSi_3O_8$ is identified at 1150 °C, 1200 and 1250 °C. The continued reaction of quartz with $LiAlSi_3O_8$ for composition C leads to the formation of $Li_xAl_xSi_{1-x}O_2$ at 1300 °C. $Li_xAl_xSi_{1-x}O_2$ appears as a stable phase and does not dissolve with increasing temperature.

The process of Li-compound formation can be described with the following reactions. The general formula for lithium aluminium silicate, $Li_xAl_xSi_{1-x}O_2$, where $x = 0$ for the keatite form of SiO_2 and 0.33 for the β-spodumene form, describes the variations in the compositions.[20] The reaction taking place between β-spodumene and quartz is described by the following equation:

$$0.75(Li_{0.33}Al_{0.33}Si_{0.67}O_2) + 0.25(SiO_2) \rightarrow Li_{0.25}Al_{0.25}Si_{0.75}O_2 \quad (1)$$

The reaction product is $Li_{0.25}\ Al_{0.25}\ Si_{0.75}O_2$, which is equivalent to $LiAlSi_3O_8$ containing more SiO_2 than β-spodumene. When derived from the general formula for lithium aluminium silicate, the above equation can be written as follows:

$$y(Li_xAl_xSi_{1-x}O_2) + (1-y)(SiO_2) \rightarrow Li_{yx}Al_{yx}Si_{1-yx}O_2 \quad (2)$$

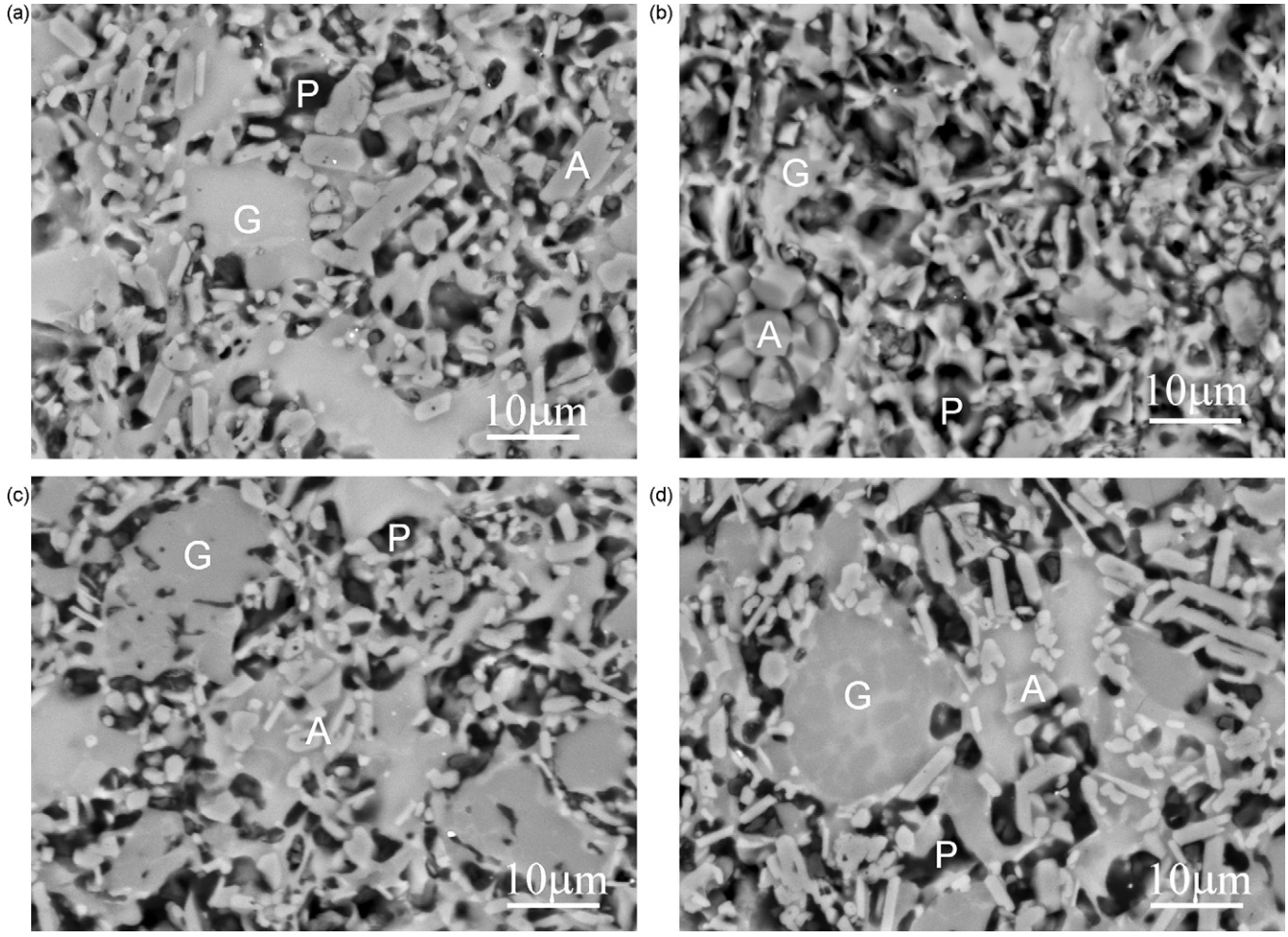

Fig. 7. SEM/BEI of samples (a) EN; (b) A; (c) B; and (d) C after firing at 1150 °C. A – corundum; G – glassy phase; P – pore.

where $y = 0.75$ and $x = 0.33$ for β-spodumene. $Li_{0.25}$ $Al_{0.25}$ $Si_{0.75}O_2$ continues to react with quartz for the same Eq. (2), except that $x = 0.25$. The final reaction product with more SiO_2 is formed.

The microstructures of samples fired at 1150 °C are shown in Fig. 7. Noticeable melting within the porous structure is observed after firing at 1150 °C for all the samples. A considerable amount of melt appears with the composition EN, because of the dissolution of its flux minerals, microcline, albite and sanidine, as confirmed by the recorded patterns of the XRD analysis, shown in Fig. 3. Liquid formation is associated with the melting of the feldspar system and the silica discarded from the metakaolin via the $K_2O-Al_2O_3-SiO_2$ eutectic,[21] indicating a feldspar and silica eutectic at 985 °C, and a eutectic between potassium feldspar, sodium feldspar and silica at 1020 °C in the system $NaAlSiO_4-KAlSiO_4-SiO_2$.[22] The melting process in the samples is clear from the DTA curves shown in Fig. 1, with the appearance of an endothermic effect that begins at around 1070 °C for all the samples.

The melting reactions in EN, where the liquid unification clearly results in separated glassy-phase regions, are more intensive than in A. Among the Li_2O-containing compositions the amount of glassy phase formed is increased with more Li_2O added, which means that C has the most glassy-phase regions, and these are surrounded by distinctive corundum grain clusters.

Fig. 8 shows the microstructures of the samples fired at 1200 °C. All the compositions underwent intensive pore closure, with an increased amount of glassy phase being formed. The microstructure of EN seems comparatively compact, but less homogeneous in terms of pores than the compositions containing Li_2O. Sample C appears to be the most vitrified, but with a relatively large amount of big, closed pores. The melted regions in the Li_2O-containing compositions are composed of darker and brighter areas, which might be the consequence of a chemical non-homogeneity of the liquid phase.

In Fig. 9 the microstructures of samples fired at 1300 °C are presented. A dense microstructure with disconnected pores is observed for all the compositions fired at this temperature. A greater uniformity of the glassy-phase distribution is observed for the samples A and B. The sizes of the glassy-phase regions in the compositions containing Li_2O are smaller than in the EN sample. In composition C, larger, spherical pores up to around 30 μm are visible, which is characteristic for an overfiring process accompanied by bloating. The liquid phase in C, owing to the relatively large amount of Li_2O, contributes a great deal to the pores joining to form larger pores.

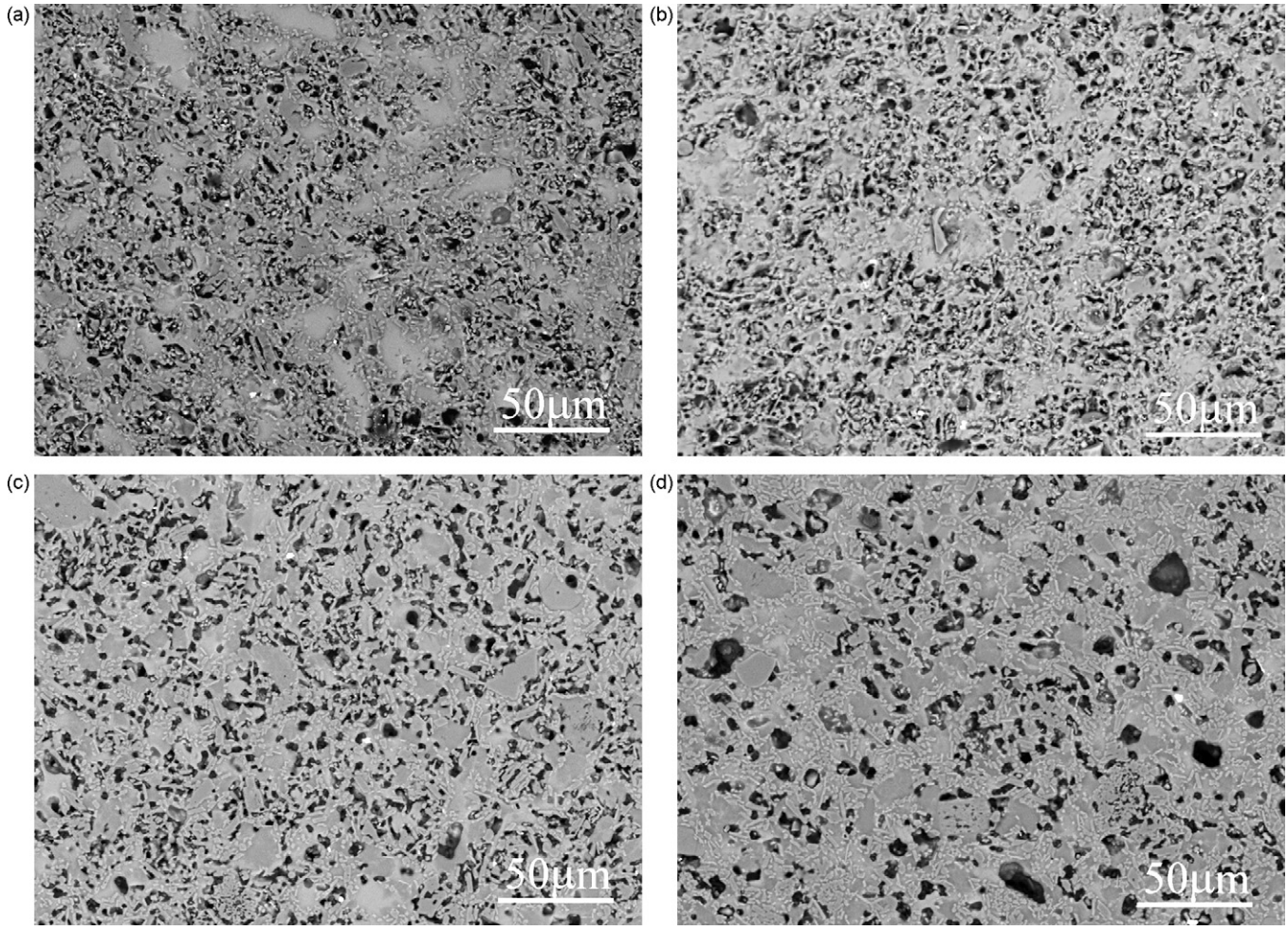

Fig. 8. SEM/BEI of samples (a) EN; (b) A; (c) B; and (d) C after firing at 1200 °C.

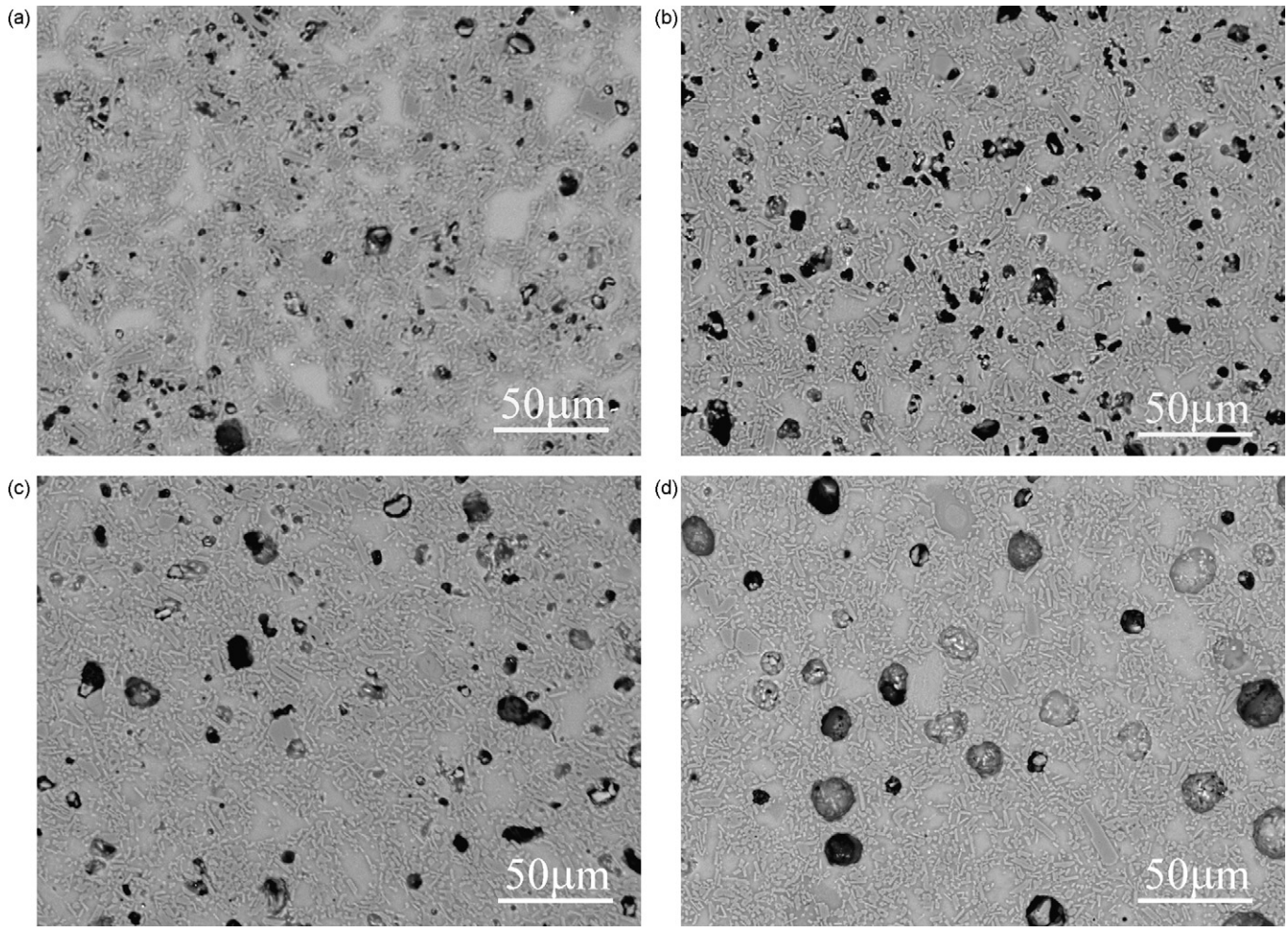

Fig. 9. SEM/BEI of samples (a) EN; (b) A; (c) B; and (d) C after firing at 1300 °C.

3.3. Physical properties of fired bodies

When the temperature is increased from 950 to 1350 °C, the colour of the fired samples changes gradually from pale brown to white for all the compositions except composition C. It appears that 1.6 wt.% of Li_2O in the alumina porcelain body leads to reactions where red compounds are formed, while with the addition of 1.0 or 1.2 wt.% there is no noticeable colour change. For the composition C the colour of the body observed on cross-sectioned surfaces changes to pale red at 1200 °C. With a temperature increase to 1250 °C several homogeneously dispersed spots of bright red appear on the surface and inside the body. At 1300 °C the colour of the body changes to a homogenous yellow-white with individual red spots in the surface, which becomes glassy. At 1350 °C there is only a slight change to a more pale-yellow, white colour with red spots remaining on the surface. Additionally, the surface appears more glassy and small bubbles are visible. All the other studied compositions develop a white homogenous appearance at 1300 and 1350 °C. The appearance of pink spots in mullite−β-spodumene composites from aluminosilicates was previously mentioned by Yamuna and Devanarayanan[13] and attributed to the pink variety of β-spodumene (kunzite), the formation of which occurs only in the presence of lithium-rich aluminosilicates and the presence of iron as an impurity in the mullite composite. When Talyaganov et al.[23] investigated the influence of Li_2O on phase transformations in formulations composed of 50 wt.% kaolin, 25 wt.% feldspar and 25 wt.% quartz, they described the appearance of pink spots in the K−Na-containing aluminosilicate matrix in compositions containing more than 2.2 wt.% Li_2O after firing at 1200 °C, which disappeared with a heat treatment at higher temperatures.

The bulk-density variations with the increasing firing temperature are plotted in Fig. 10. The Li_2O-containing samples thicken more intensively in the temperature range 1150–1250 °C in comparison to EN, as is evident from the slope of the corresponding graphs. At 1300 °C the samples EN, A and B attain their maximum bulk densities. The composition C attains its maximum bulk density at 1250 °C, which is 50 °C lower than for the other compositions, showing that an increased amount of Li_2O contributes to a densification process at lower temperatures. The overfiring effect is noticeable at 1350 °C for the samples EN and B, while an exaggerated overfiring effect appears for sample C even at 1300 °C. However, no overfiring effect was noticeable for sample A. The presence of 1.0 wt.% of Li_2O is the most favourable with regard to samples prone to overfiring.

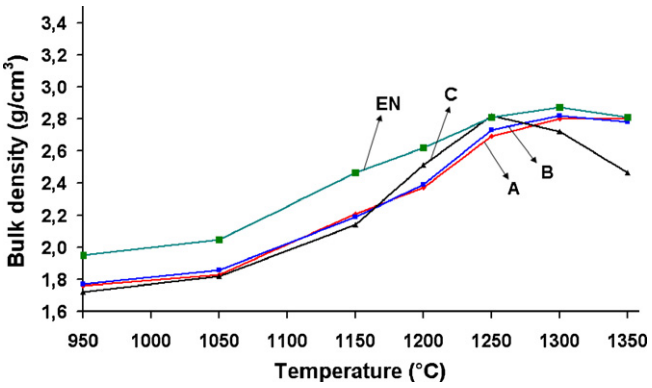

Fig. 10. Bulk density of studied compositions fired in the temperature range 950–1350 °C.

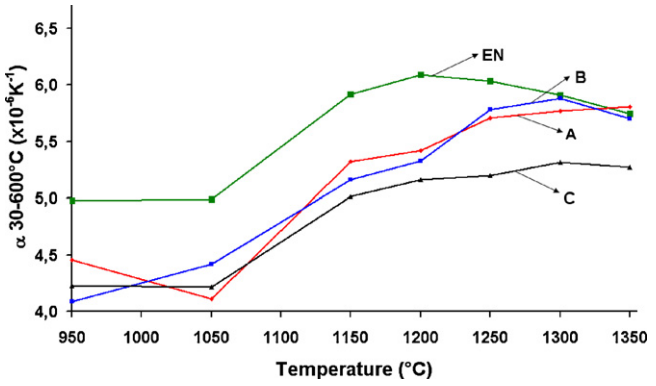

Fig. 12. Coefficient of thermal expansion in temperature interval 30–600 °C of studied compositions fired in the temperature range 950–1350 °C.

Fig. 11 shows the open porosity of samples fired at different temperatures. Samples EN, B and C have no open porosity at 1250 °C, while sample A still has 2 vol.% of open porosity. For sample A, zero open porosity is reached at 1300 °C. The pore closing in the temperature range 1150–1200 °C is most clearly seen for sample C, as is evident from the greater slope of the corresponding curve, and which agrees with the SEM observations in Fig. 8, where the highest amount of glassy phase is observed for sample C at 1200 °C. Intensive pore elimination is observed for all the samples in the temperature range 1200–1250 °C.

The influence of firing temperature on the thermal expansion of fired bodies is shown in Fig. 12, where the graphs of the CTE in the temperature range 30–600 °C are plotted. A and B have a lower CTE than EN when fired below 1300 °C, whereas the CTE of A and B is similar to that of EN for the samples fired at 1300 and 1350 °C, with the value $\sim 5.8 \times 10^{-6}\ K^{-1}$. The composition C has a considerably lower CTE than the other compositions in the firing range 1150–1350 °C, which is correlated with the amount of Li-containing phases present on the basis of XRD studies. Lithium aluminium silicates are characterized by a low overall thermal expansion.[24]

The influence of the firing temperature on the flexural strength is shown in Fig. 13. The flexural strength of the EN samples gradually increases up to 190 MPa at 1350 °C. The Li-containing samples attain their maximum flexural strength at 1300 °C, with values of 203, 204 and 127 MPa for A, B and C, respectively. The maximum flexural strength of A and B is higher than that of EN. Above 1300 °C the decreasing of the flexural strength is determined by A, B and C. A and B have similar flexural strengths across the entire firing range. The flexural strength of C is comparable to that of A and B for the samples fired up to 1200 °C, while this strength is notably lower for the samples fired at 1250 °C and above.

At 1300 °C A, B and EN achieve their maximum bulk densities, but the coinciding of the maximum flexural strength and the maximum bulk density is observed only for A and B. Both C and EN attain a higher flexural strength at temperatures above their maximum bulk density.

The mechanical strength in a multiphase porcelain body strongly depends on the firing process, which affects the main factors influencing the strength, such as the thermal expansion coefficient of the phases, the elastic properties of the phases, the volume fractions of the various phases, the particle size of the crystalline phase, and the phase transformation, which all contribute to the stresses configuration in the glassy matrix.[1] It was shown that the mechanical strength of porcelain is mainly influenced by the pre-stresses induced between the glassy matrix and the crystalline material with a higher thermal expansion than that of the glassy matrix.[25] The higher flexural strength of A and B in comparison to EN at 1300 °C may be partially attributed to the lower thermal expansion of the glassy phases of A and B, containing Li_2O, since for A and B a slightly lower CTE was determined at this temperature.

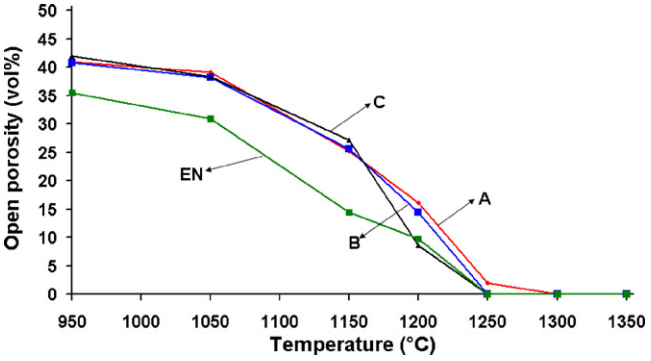

Fig. 11. Open porosity of studied compositions fired in the temperature range 950–1350 °C.

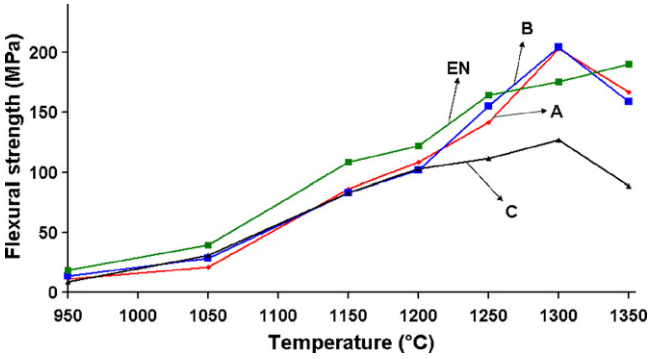

Fig. 13. Flexural strength of studied compositions fired in the temperature range 950–1350 °C.

Table 2
Bulk density, coefficient of thermal expansion, flexural strength and thermal shock resistance at $\Delta T = 200\,^{\circ}C$ of studied compositions fired at 1315 °C/1 h in gas kiln.

Composition	Bulk density (g/cm^3)	CTE 20–600 °C ($\times 10^{-6}$ K^{-1})	Flexural strength (MPa)	Thermal shock resistance at $\Delta T = 200\,^{\circ}C$
EN[a]	2.91	5.83	194	No
A	2.85	5.69	204	Yes
B	2.91	5.57	202	Yes
C	2.74	5.63	154	Yes

[a] Average year value under industrial conditions.

On the other hand, at 1300 °C composition C achieves its maximum flexural strength, which is significantly lower than all the other the compositions. The lower strength of C might be partially ascribed to the presence of the low-expansion lithium aluminosilicate crystalline phase, as identified in the XRD spectra. The literature suggests that the strength reduction of a porcelain body is induced by the presence of flaws and inhomogeneities consisting of grains with a thermal expansion lower than the body.[25]

After firing at 1350 °C, the flexural strength of the Li_2O-containing compositions decreases remarkably. This decrease of the flexural strength is influenced by the bloating phenomena, as seen in the corresponding sintering curves and the bulk density increase at 1350 °C. Due to the bloating phenomena the increase in the closed pores negatively affects the elastic modulus and the strength.[26]

The presence of residual quartz in the EN composition, as identified from the XRD patterns of EN at 1300 and 1350 °C, has a negative influence on its flexural strength. Large quartz grains negatively affect the strength of the porcelain body, since they cause cracks in the vitreous phase.[27] Reversible quartz inversion from β to α at 573 °C during the cooling process, accompanied by a volume decrease, is responsible for the deterioration in the mechanical properties of the body.[28]

3.4. Firing in the gas kiln

Test samples of the studied compositions were additionally fired in a gas kiln with a maximum temperature of 1315 °C. After firing, all the samples exhibited zero open porosity. In Table 2 the bulk density, the CTE in the temperature range 20−600 °C, the flexural strength and the thermal shock resistance at $\Delta T = 200\,^{\circ}C$ of the fired samples are indicated. Samples A, B and EN attain higher bulk densities in comparison to the maximum bulk densities achieved by firing in a laboratory furnace. The samples containing Li_2O have a similar CTE, which is lower than for EN. The determined flexural strength is 204 MPa for A, 202 MPa for B and 194 MPa for EN, while a considerably lower value of 154 MPa was obtained for C. Samples A, B and C show equal thermal shock resistance at $\Delta T = 200\,^{\circ}C$, with cracks appearing in two of the five samples after water quenching, while all five EN samples experienced cracks. The thermal shock resistance of the samples fired in the gas kiln is improved with the introduction of Li_2O.

The deformation during firing in a gas kiln, measured as a distortion of the fired samples, is 16 mm for EN, 14 mm for A, 22 mm for B and much greater for C, with the test bars falling off the supports. Deformation during firing is an important criterion for the industrial application of a newly developed body. The requirement for sufficient vitrification and low pyroplastic deformation is one of the main compromises in the design of a firing schedule for a porcelain body.[7] Deformation during the firing of the Li_2O-containing bodies is most significant for A when fired under the existing firing schedule in the gas kiln.

4. Conclusions

Li_2O was introduced in amounts of 1.0, 1.2 and 1.6 wt.% in high-alumina porcelain bodies with ∼61 wt.% of Al_2O_3 via β-spodumene. The phase composition and the microstructure evolution of the standard composition and the Li_2O-containing compositions were studied in the firing-temperature range 950−1350 °C.

Li_2O-bearing compositions reach a higher degree of densification at lower temperatures in comparison to the reference composition. The influence on the densification is greater, with the amount of Li_2O increasing. During heat treatment the phase composition of the bodies is influenced by the amount of added Li_2O. It is evident that the reduction of quartz in the presence of Li_2O in the temperature range 1150−1250 °C is due to the quartz's reaction with β-spodumene, forming $LiAlSi_3O_8$. The reaction of quartz is promoted by the increased amount of Li_2O. The continued reaction of quartz at higher temperatures leads to the formation $Li_xAl_xSi_{1-x}O_2$, when the amount of Li_2O is 1.6 wt.%. The presence of lithium minerals contributes to the lower CTE of bodies containing Li_2O.

Homogeneity of the microstructure, a high bulk density and an improved flexural strength are exhibited by compositions with 1.0 and 1.2 wt.% of Li_2O fired at1300 °C. When fired at higher temperatures all the compositions containing Li_2O attain a noticeably lower flexural strength, mainly due to the bloating phenomena, which increases with the increasing amount of Li_2O, as is obvious from the decreasing bulk density.

The increasing amount of Li_2O greatly affects the deformation during firing in the industrial kiln, which considerably increases with the increasing amount of Li_2O. Under the existing firing schedule in the industrial kiln the most favourable characteristics from an industrial perspective are attained by the composition with 1.0 wt.% Li_2O.

Our investigations of Li_2O as the main flux constituent in high-alumina porcelain bodies showed that Li_2O is a strong fluxing agent that contributes to achieving a high mechanical strength and good thermal shock resistance, which strongly depend on the amount of Li_2O and the firing conditions.

Acknowledgements

The authors would like to thank to Mrs. Helena Razpotnik, Mrs. Lidija Sopotnik and Mrs. Joži Prašnikar from ETI Elektroelement d.d., and Mrs. Jena Cilenšek and Mr. Silvo Drnovšek from Institute Jožef Stefan, Electronic Ceramics Department, for their assistance in the experimental work.

References

1. Carty, W. M. and Senapati, U., Porcelain—raw materials, processing, phase evolution, and mechanical behavior. *J. Am. Ceram. Soc.*, 1998, **81**, 3–20.
2. Liebermann, J., Microstructure properties and product quality of strength-stressed high-voltage insulators. *Am. Ceram. Soc. Bull.*, 2003, **82**, 39–46.
3. Amigó, J. M., Clausell, J. V., Esteve, V., Delgado, J. M., Reventós, M. M., Orchando, L. E. *et al.*, X-ray powder diffraction phase analysis and thermo-mechanical properties of silica and alumina porcelains. *J. Eur. Ceram. Soc.*, 2004, **24**, 75–81.
4. Liebermann, J. and Schulle, W., *Bauxite Porcelain. Am. Ceram. Soc. Bull.*, 2002, **81**, 33–38.
5. Lee, W. E., Souza, G. P., McConville, C. J., Tarvornpanich, T. and Iqbal, Y., Mullite formation in clays and clay-derived vitreous ceramics. *J. Eur. Ceram. Soc.*, 2008, **28**, 465–471.
6. Kristoffersson, A., Ekberg, I. L., Leandersson, H. and Carlsson, R., High strength triaxial porcelain by an improved glassy phase. In *Proceeding of the third euro-ceramics, 2*, 1993, pp. 1059–1064.
7. Villegas-Palacio, S. and Dinger, D. R., PSD effects on firing properties of porcelains. *I. Am. Ceram. Soc. Bull.*, 1996, **75**, 71–76.
8. Cowan, C. A., Bole, G. A. and Stone, R. L., Spodumene as a flux component in sanitary chinaware bodies. *J. Am. Ceram. Soc.*, 1950, **33**, 193–197.
9. Ismatova, R., Properties and structure of spodumene-porcelain. *Steklo i keramika*, 1987, **7**, 27–28.
10. Tulyaganov, D. U., Agathopoulos, S., Fernandes, H. R. and Ferreira, J. M. F., Influence of lithium oxide as auxiliary flux on the properties of triaxial porcelain bodies. *J. Eur. Ceram. Soc.*, 2006, **26**, 1131–1139.
11. Tucci, A., Esposito, L., Malmusi, L. and Rambaldi, E., New body mixes for porcelain stoneware tiles with improved mechanical characteristics. *J. Eur. Ceram. Soc.*, 2007, **27**, 1875–1881.
12. Low, I. M., Mathews, E., Garrod, T., Zhou, D., Phillips, D. N. and Pillai, X. M., Processing of spodumene-modified mullite ceramics. *J. Mater. Sci.*, 1997, **32**, 3807–3812.
13. Yamuna, A. and Devanarayanan, S., Mullite-β-spodumene composites from aluminosilicates. *J. Am. Ceram. Soc.*, 2001, **84**, 1703–1709.
14. Bayuseno, A. P., Latella, B. A. and O'Connor, B. H., Resistance of alumina-spodumene ceramics to thermal shock. *J. Am. Ceram. Soc.*, 1999, **82**, 819–824.
15. IEC 60672-2, *Ceramic and Glass-Insulating Materials, Part 2. Methods of Test*. International Electrotechnical Commission, Geneva, CH, 1999.
16. Gualtieri, A. F., Thermal behavior of the raw materials forming porcelain stoneware mixtures by combined optical and *in situ* X-ray dilatometry. *J. Am. Ceram. Soc.*, 2007, **90**, 1222–1231.
17. Lee, S., Kim, Y. J. and Moon, H.-S., Phase transformation sequence from kaolinite to mullite investigated by an energy-filtering transmission electron microscope. *J. Am. Ceram. Soc.*, 1999, **82**, 2841–2848.
18. Iqbal, Y. and Lee, W. E., Fired porcelain microstructures revisited. *J. Am. Ceram. Soc.*, 1999, **82**, 3584–3590.
19. Iqbal, Y. and Lee, W. E., Microstructural evolution in triaxial porcelain. *J. Am. Ceram. Soc.*, 2000, **83**, 3121–3127.
20. Subramanian, M. A., Corbin, D. R. and Farlee, R. D., X-ray and MAS NMR characterization of the thermal transformation of Li(Na)-Y zeolite to lithium aluminosilicates. *Mater. Res. Bull.*, 1986, **21**, 1525–1532.
21. The American Ceramic Society and National Institute of Standards and Technology, Phase Equilibria Diagrams, CD-ROM, Database, Version 3.0. Vol. 01, Fig 00407.
22. The American Ceramic Society and National Institute of Standards and Technology, Phase Equilibria Diagrams, CD-ROM, Database, Version 3.0. Vol. 01, Fig 00786.
23. Talyaganov, D. U., Agathopoulos, S., Fernandes, H. R., Ferreira, J. M. F. and Fabrichnaya, O., Influence of Li_2O doping on non-isothermal evolution of phases in K-Na-containing aluminosilicate matrix. *J. Am. Ceram. Soc.*, 2006, **89**, 292–297.
24. Ostertag, W., Fischer, G. R. and Williams, J. P., Thermal expansion of synthethic β-spodumene—silica solid solutions. *J. Am. Ceram. Soc.*, 1968, **51**, 651–654.
25. Mattyasovszky-Zsolnay, L., Mechanical strength of porcelain. *J. Am. Ceram. Soc.*, 1957, **40**, 299–306.
26. Kobayashi, Y., Ohira, O., Ohashi, Y. and Kato, E., Effect of firing temperature on bending strength of porcelains for tableware. *J. Am. Ceram. Soc.*, 1992, **75**, 1801–1806.
27. Ece, O. I. and Nakagawa, Z., Bending strength of porcelains. *Ceram. Int.*, 2002, **28**, 131–140.
28. Warshaw, S. I. and Seider, R., Comparison of strength of triaxial porcelains containing alumina and silica. *J. Am. Ceram. Soc.*, 1967, **50**, 337–343.